47th AIAA Aerospace Sciences Meeting Including The New Horizons Forum and Aerospace Exposition
5 - 8 January 2009, Orlando, Florida

AIAA 2009-1312

Simulation of Flows at All Speeds with Implicit High-Order WENO Schemes

Yiqing Shen*, Gecheng Zha†
Dept. of Mechanical and Aerospace Engineering
Miami Wind ^{TM}
University of Miami
Coral Gables, Florida 33124
E-mail: yqshen@miami.edu, gzha@miami.edu

Abstract

In this paper, an unified high-order algorithm for all speeds is developed. The preconditioning matrix of Weiss and Smith combined with a 5th-order WENO scheme for inviscid flux and a fully conservative 4th order central differencing for viscous terms are employed. The unfactored implicit Gauss-Seidel relaxation scheme is used for time marching. The numerical simulation of a natural convective cavity flow, subsonic flow, transonic and supersonic flows show that the high order preconditioning method is efficient, robust, and accurate for both low speed incompressible flows and high speed compressible flows.

1 Introduction

In recent years, there is a growing interest to develop an unified algorithm for compressible and incompressible flows in computational fluid dynamics (CFD) for two reasons: First, there exist flow problems of mixed compressible/incompressible type. Second, it is convenient to use the same CFD code for pure incompressible or compressible flows. For example, the design of an aircraft or a launch vehicle involves the calculation of flows during a full flight mission passing through various flow regimes[1]. The other example of co-existing incompressible and compressible flow is the ship-aircraft dynamic interface[2], where the flow near ship deck is low speed incompressible flow, and the flow around aircraft is compressible due to helicopter rotor tip speed and high speed engine nozzle jet.

The system of compressible flow governing equations at very low Mach numbers is stiff due to the large ratio of the acoustic and convective time scales, or the large disparity in acoustic wave speed, $u + a$, and the waves convected at fluid speed, u. That is, there exists a large difference in the eigenvalues of the convective flux Jacobians when the incompressible limit is approached. The largest eigenvalue tends to approach the speed of sound, whereas the smallest eigenvalue approaches zero. The large difference of the eigenvalues will exacerbate the condition numbers of the linearized system and create the analytical stiffness[3].

In addition to the stiffness problem, the other issue of direct applying compressible flow equation to incompressible flows is that the numerical dissipation is large at stagnation points. This is again because

* Research Scientist, AIAA Member
† Associate Professor, AIAA Senior Member

of the large difference between the speed of sound and flow speed. The large dissipation may distort the solution of a wall boundary layer.

Preconditioning is to change the eigenvalues of the compressible flow equations system in order to remove the large disparity of wave speeds. Usually, the system of compressible flow equations is preconditioned by multiplying the time derivatives with a suitable matrix[4, 5, 6, 7, 8]. In recent years, considerable progress has been made in the development of preconditioning methods for accelerating the convergence of Euler and Navier-Stokes solvers at low Mach numbers. An excellent review is given by Turkel in [9]. The preconditioning methods have been used to conduct the large-eddy simulations of turbulent channel flows and cylinder flows[10], the turbulent pipe flows[11], the turbulent flows over an airfoil and wing at subsonic and transonic conditions[12], nonequilibrium condensate flows in a nozzle[13].

For the spatial discretization with preconditioning, the 2nd order central differencing is adopted by Choi and Merkle [7, 14] and Bortoli[1]. The Roe-type flux-difference splitting (FDS) is used by Weiss and Smith [8, 15, 16]. The third-order MUSCL extrapolation is used by Briley et al [17]. The flux-vector splitting (FVS) is applied by Turkle et al [18]. Edwards and Liu[19] have extended the advective upwind splitting method (AUSM) to all flow speeds. Nigro et al[20] combined the preconditioning mass matrix[7] with an SUPG finite element formulation. Rossow[21] developed a blended pressure/density based approach, the MAPS+ flux scheme in terms of Mach number. All these preconditioned methods employ 2nd order schemes.

Many engineering applications may have discontinuities in the flows such as shock waves or contact surfaces. The essentially non-oscillatory (ENO) or weighted essentially non-oscillatory (WENO) schemes are attractive for their capability to capture discontinuities and achieve the consistent high order accuracy in smooth regions. By using a convex combination of all candidate stencils to replace the smoothest one in the ENO scheme, a WENO scheme has more advantages over its ENO counterpart. For example, it approaches certain high order accuracy in smooth regions and has better convergence due to the smoother numerical flux used. From its appearance [22, 23] to present, the WENO schemes have been extensively applied to different flow problems in many areas. Engineering problems often have the compressible and incompressible flow regimes existing simultaneously, including shock wave and contact surface (e.g. air/water interface). To improve the simulation accuracy, it is very desirable to apply high order ENO/WENO schemes with preconditioning to treat the complicated flows at all speed.

The implicit methods for compressible flow calculation have been widely employed due to their less stiffness and faster convergence rate than the explicit schemes. The unfactored implicit Gauss-Seidel relaxation scheme avoids the factorization error introduced by the approximate factoritation (AF) implicit schemes and the lower-upper symmetric Gauss-Seidel (LU-SGS) method, and hence has larger time steps with faster convergence rate[24, 25, 26, 27].

In this paper, a preconditioned 5th-order WENO scheme with the unfactored implicit Gauss-Seidel relaxation scheme is developed to simulate the flows at all speeds. To our knowledge, this appears to be the first effort to apply a high order WENO scheme with preconditioning. Several flows from very low speed to supersonic speed are calculated with the present methodology to demonstrate its robustness, accuracy, and efficency.

2 Governing Equations

The normalized Navier-Stokes equations governing compressible viscous flows can be written in the Cartesian coordinate as:

$$\frac{\partial Q}{\partial t}+\frac{\partial E}{\partial x}+\frac{\partial F}{\partial y}+\frac{\partial G}{\partial z}=\frac{1}{Re}\left(\frac{\partial R}{\partial x}+\frac{\partial S}{\partial y}+\frac{\partial T}{\partial z}\right) \tag{1}$$

where

$$Q = \begin{bmatrix} \rho \\ \rho u \\ \rho v \\ \rho w \\ \rho e \end{bmatrix}, E = \begin{bmatrix} \rho u \\ \rho u^2 + p \\ \rho uv \\ \rho uw \\ (\rho e + p)u \end{bmatrix}, F = \begin{bmatrix} \rho v \\ \rho uv \\ \rho v^2 + p \\ \rho vw \\ (\rho e + p)v \end{bmatrix}, G = \begin{bmatrix} \rho w \\ \rho uw \\ \rho vw \\ \rho w^2 + p \\ (\rho e + p)w \end{bmatrix},$$

$$R = \begin{bmatrix} 0 \\ \tau_{xx} \\ \tau_{xy} \\ \tau_{xz} \\ u_k\tau_{xk} - q_x \end{bmatrix}, S = \begin{bmatrix} 0 \\ \tau_{xy} \\ \tau_{yy} \\ \tau_{yz} \\ u_k\tau_{yk} - q_y \end{bmatrix}, T = \begin{bmatrix} 0 \\ \tau_{xz} \\ \tau_{yz} \\ \tau_{zz} \\ u_k\tau_{zk} - q_z \end{bmatrix},$$

The repeated index k stands for the Einstein summation over x, y and z. The stress τ and heat flux q are,

$$\tau_{ik} = (\mu + \mu_t)\left[(\frac{\partial u_i}{\partial x_k} + \frac{\partial u_k}{\partial x_i}) - \frac{2}{3}\delta_{ik}\frac{\partial u_j}{\partial x_j}\right]$$

$$q_j = \frac{-1}{(\gamma - 1)M_\infty^2}(\frac{\mu}{Pr} + \frac{\mu_t}{Pr_t})\frac{\partial T}{\partial x_j}$$

The equation of state is

$$\rho e = \frac{p}{\gamma - 1} + \frac{1}{2}\rho(u^2 + v^2 + w^2)$$

where μ_t is the turbulence eddy viscosity calculated by Baldwin-Lomax(BL) model[28].

In the above equations, ρ is the density, u, v, and w are the Cartesian velocity components in x, y and z directions, p is the static pressure, and e is the total energy per unit mass, μ is the molecular viscosity, J is the transformation Jacobian, $\gamma, Re, M_\infty, Pr\ and\ Pr_t$ are the ratio of specific heat, Reynolds number, freestream Mach number, Prandtl number and turbulent Prandtl number, respectively.

The dimensionless flow variables in the governing equations are defined as the following,

$$x^* = \frac{x}{L}, y^* = \frac{y}{L}, z^* = \frac{z}{L},$$

$$u^* = \frac{u}{U_\infty}, v^* = \frac{v}{U_\infty}, w^* = \frac{w}{U_\infty},$$

$$\rho^* = \frac{\rho}{\rho_\infty}, \mu^* = \frac{\mu}{\mu_\infty}, t^* = \frac{t}{L/U_\infty},$$

$$T^* = \frac{T}{T_\infty}, p^* = \frac{p}{\rho_\infty U_\infty^2}, e^* = \frac{e}{U_\infty^2}, \mu^* = \frac{\mu}{\mu_\infty}$$

where L is the reference length, the free stream conditions are denoted by the subscript ∞. For simplicity, the subscript * is omitted in Eq.(1). In the generalized coordinates, Eq.(1) can be written as:

$$\frac{\partial Q'}{\partial t} + \frac{\partial E'}{\partial \xi} + \frac{\partial F'}{\partial \eta} + \frac{\partial G'}{\partial \zeta} = \frac{1}{Re}\left(\frac{\partial R'}{\partial \xi} + \frac{\partial S'}{\partial \eta} + \frac{\partial T'}{\partial \zeta}\right) \tag{2}$$

where,

$$Q' = \frac{1}{J}Q,$$

$$E' = \frac{1}{J}(\xi_t Q + \xi_x E + \xi_y F + \xi_z G),$$
$$F' = \frac{1}{J}(\eta_t Q + \eta_x E + \eta_y F + \eta_z G),$$
$$G' = \frac{1}{J}(\zeta_t Q + \zeta_x E + \zeta_y F + \zeta_z G),$$
$$R' = \frac{1}{J}(\xi_x R + \xi_y S + \xi_z T),$$
$$S' = \frac{1}{J}(\eta_x R + \eta_y S + \eta_z T),$$
$$T' = \frac{1}{J}(\zeta_x R + \zeta_y S + \zeta_z T).$$

For simplicity, the prime $'$ in Eq.(2) will be omitted in the rest of this paper.

3 Preconditioned System

The preconditioned system for steady state flows in conservative form is obtained by multiplying the preconditioning matrix Γ to the time derivative terms of Eq.(2) to give

$$\Gamma \frac{\partial q}{\partial t} + \frac{\partial E}{\partial \xi} + \frac{\partial F}{\partial \eta} + \frac{\partial G}{\partial \zeta} = \frac{1}{Re}\left(\frac{\partial R}{\partial \xi} + \frac{\partial S}{\partial \eta} + \frac{\partial T}{\partial \zeta}\right) \tag{3}$$

The preconditioning matrix Γ has various forms[4, 6, 7, 8], and is dependent on the choice of q. This paper adopts the method of Weiss and Smith described in Ref.[8]. The q and Γ are taken as the following,

$$q = (p, u, v, w, T)^T$$

$$\Gamma = \begin{bmatrix} \Theta & 0 & 0 & 0 & \rho_T \\ \Theta u & \rho & 0 & 0 & \rho_T u \\ \Theta v & 0 & \rho & 0 & \rho_T v \\ \Theta w & 0 & 0 & \rho & \rho_T w \\ \Theta H - 1 & \rho u & \rho v & \rho w & \rho_T H + \rho C_p \end{bmatrix}$$

where Θ is given by

$$\Theta = (\frac{1}{U_r^2} - \frac{\rho_T}{\rho C_p})$$

U_r is a reference velocity. In this paper, the reference velocity proposed by Edwards and Roy[19] is used:

$$U_r = min[c, max(|V|, k|V_\infty|)]$$

where, c is the speed of sound, $|V| = \sqrt{u^2 + v^2 + w^2}$ is the velocity magnitude, $|V_\infty|$ is a reference velocity. H is the total enthalpy, ρ_T stands for $\frac{\partial \rho}{\partial T}$, C_p is the specific heat at constant pressure. k is a constant and $k = 0.5$ is used in this paper.

4 Flux Difference Splitting and WENO Scheme

The Roe's flux difference scheme [29] is used as the Riemann solver for the WENO scheme in this paper. For the rest of the paper, we will take the flux in ξ direction as the example to explain the numerical methodology. Other directions can be obtained following the symmetric rule.

The preconditioned Roe scheme can be expressed as the following[8]:

$$E_{i+\frac{1}{2}} = \frac{1}{2}[E(q^L) + E(q^R) - \tilde{A}(q^R - q^L)]_{i+\frac{1}{2}} \tag{4}$$

where

$$\tilde{A} = \Gamma M_\Gamma |\Lambda_\Gamma| M_\Gamma^{-1}$$

The subscript Γ denotes that the diagonal matrix of eigenvalues and the eigenvector matrix are derived from the preconditioned system.

$$\Lambda_\Gamma = diag(U, U, U, U' + C', U' - C')$$

$$M_\Gamma = \begin{bmatrix} 0 & 0 & 0 & 1 & 1 \\ 0 & \eta_x & \zeta_x & \frac{-\xi_x}{X_1} & \frac{-\xi_x}{X_2} \\ 0 & \eta_y & \zeta_y & \frac{-\xi_y}{X_1} & \frac{-\xi_y}{X_2} \\ 0 & \eta_z & \zeta_z & \frac{-\xi_z}{X_1} & \frac{-\xi_z}{X_2} \\ 1 & 0 & 0 & X_3 & X_4 \end{bmatrix}$$

$$M_\Gamma^{-1} = \begin{bmatrix} \frac{1}{X_5} & \frac{\xi_x X_6}{X_5} & \frac{\xi_x X_6}{X_5} & \frac{\xi_x X_6}{X_5} & 1 \\ 0 & \eta_x & \eta_y & \eta_z & 0 \\ 0 & \zeta_x & \zeta_y & \zeta_z & 0 \\ -\frac{\tilde{U}\alpha - \tilde{C}'}{2\tilde{C}'} & -\xi_x X_7 & -\xi_y X_7 & -\xi_z X_7 & 0 \\ \frac{\tilde{U}\alpha + \tilde{C}'}{2\tilde{C}'} & \xi_x X_7 & \xi_y X_7 & \xi_z X_7 & 0 \end{bmatrix}$$

and

$$U = \xi_x u + \xi_y v + \xi_z w$$

$$U' = U(1-\alpha),\ C' = \sqrt{\alpha^2 U^2 + (\xi_x^2 + \xi_y^2 + \xi_z^2) U_r^2}$$

$$\alpha = (1 - \beta U_r^2)/2,\ \beta = \rho_p + \frac{\rho_T}{\rho C_p}$$

$$X_1 = \rho(\tilde{U}\alpha - \tilde{C}')$$

$$X_2 = \rho(\tilde{U}\alpha + \tilde{C}')$$

$$X_3 = \frac{1 - (\rho_p - \Theta)\tilde{U}(\tilde{U}\alpha - \tilde{C}')}{(\rho_T + \rho C_p \Theta)(\tilde{U}\alpha - \tilde{C}')^2}$$

$$X_4 = \frac{1 - (\rho_p - \Theta)\tilde{U}(\tilde{U}\alpha + \tilde{C}')}{(\rho_T + \rho C_p \Theta)(\tilde{U}\alpha + \tilde{C}')^2}$$

$$X_5 = (\rho_T + \rho C_p \Theta)(\tilde{U}^2\alpha^2 - \tilde{C}'^2)$$

$$X_6 = \rho\tilde{U}[2\alpha - (\rho_p - \Theta)(\tilde{U}^2\alpha^2 - \tilde{C}'^2)]$$

$$X_7 = \frac{\rho(\tilde{U}^2\alpha^2 - \tilde{C}'^2)}{2\tilde{C}'}$$

The analysis in the generalized coordinates is similar to that in Cartesian coordinates as given in Ref.[8]. For an ideal gas, $\beta = (\gamma RT)^{-1} = 1/c^2$. Thus, when $U_r = c$, $\alpha = 0$, and the eigenvalues of the preconditioned system take their original form $U \pm c\sqrt{\xi_x^2 + \xi_y^2 + \xi_z^2}$ for compressible flows. At low speed, as $U_r \to 0$, $\alpha \to \frac{1}{2}$, all the eigenvalues become the same order as U.

The high order accuracy of $E_{i+1/2}$ is obtained by achieving the high order accuracy of the left and right

conservative variables q^L and q^R using the WENO scheme described below. This procedure is similar to the MUSCL scheme suggested by van Leer[30] and is adopted in [31].

The finite difference 5th-order accuracy WENO scheme suggested by Jiang and Shu [23] is used to evaluate the conservative variables q^L and q^R. The WENO scheme for variable q^L can be written as:

$$q^L_{i+1/2} = \omega_0 q_0 + \omega_1 q_1 + \omega_2 q_2 \tag{5}$$

where ω_0, ω_1 and ω_2 are the weights, and the q_0, q_1 and q_2 are the 3rd order accuracy reconstruction of the variables in three different stencils. They are determined as the following,

$$q_0 = \frac{1}{3}q_{i-2} - \frac{7}{6}q_{i-1} + \frac{11}{6}q_i$$

$$q_1 = -\frac{1}{6}q_{i-1} + \frac{5}{6}q_i + \frac{1}{3}q_{i+1}$$

$$q_2 = \frac{1}{3}q_i + \frac{5}{6}q_{i+1} - \frac{1}{6}q_{i+2}$$

and

$$\omega_k = \frac{\alpha_k}{\alpha_0 + \cdots + \alpha_{r-1}}, \tag{6}$$

$$\alpha_k = \frac{C_k}{(\varepsilon + IS_k)^p}, \quad k = 0, 1, 2 \tag{7}$$

where C_k are the optimal weights with the following values:

$$C_0 = 0.1, \quad C_1 = 0.6, \quad C_2 = 0.3$$

The IS_k are the smooth estimators determined as

$$\begin{array}{l} IS_0 = \frac{13}{12}(q_{i-2} - 2q_{i-1} + q_i)^2 + \frac{1}{4}(q_{i-2} - 4q_{i-1} + 3q_i)^2 \\ IS_1 = \frac{13}{12}(q_{i-1} - 2q_i + q_{i+1})^2 + \frac{1}{4}(q_{i-1} - 4q_i + 3q_{i+1})^2 \\ IS_2 = \frac{13}{12}(q_i - 2q_{i+1} + q_{i+2})^2 + \frac{1}{4}(q_i - 4q_{i+1} + 3q_{i+2})^2 \end{array} \tag{8}$$

The ε in Eq.(7) is introduced to avoid the denominator becoming zero. Jiang and Shu's numerical tests indicate that the results are not sensitive to the choice of ε as long as it is in the range of 10^{-5} to 10^{-7}. In their paper[23], ε is taken as 10^{-6}. In Ref. [31], the ε value of 10^{-2} suggested to surpress the oscillation of IS_k and improve the convergence and accuracy is adopted in this paper.

The u^R is constructed symmetrically as q^L about $i + 1/2$.

4.1 The 4th-Order Schemes for Viscous Terms[31, 32]

A set of fully conservative 4th-order accurate finite central differencing schemes using the same stencil width of the WENO scheme for the viscous terms is used in this paper. The scheme for the viscous derivative term $\frac{\partial R}{\partial \xi}$ in Navier-Stokes equations Eq.(2) can be written as the following,

$$\frac{\partial R}{\partial \xi}|_i = \frac{\tilde{R}_{i+1/2} - \tilde{R}_{i-1/2}}{\Delta \xi} \tag{9}$$

To obtain 4th order accuracy, $\tilde{R}$ needs to be reconstructed as

$$\tilde{R}_{i-1/2} = \sum_{I=i-3/2}^{i+1/2} \alpha_I R_I \tag{10}$$

where

$$\begin{aligned}
\alpha_{i-3/2} = -\frac{1}{24},\ \alpha_{i-1/2} = \frac{26}{24},\ \alpha_{i+3/2} = -\frac{1}{24} \\
R_{i-1/2} = \left[(\xi_x \tau_{xx}) + (\eta_y \tau_{xy}) + (\zeta_z \tau_{xz})\right]_{i-1/2} \\
\begin{aligned}
(\tau_{xx}) = \ & \mu\{\tfrac{4}{3}\left[(\xi_x \tfrac{\partial u}{\partial \xi}) + (\eta_x \tfrac{\partial u}{\partial \eta}) + (\zeta_x \tfrac{\partial u}{\partial \zeta})\right] \\
& -\tfrac{2}{3}[(\xi_y \tfrac{\partial v}{\partial \xi}) + (\eta_y \tfrac{\partial v}{\partial \eta}) + (\zeta_y \tfrac{\partial v}{\partial \zeta}) \\
& (\xi_z \tfrac{\partial w}{\partial \xi}) + (\eta_z \tfrac{\partial w}{\partial \eta}) + (\zeta_z \tfrac{\partial w}{\partial \zeta})]\}
\end{aligned}
\end{aligned} \tag{11}$$

If R_I in Eq.(10) can be approximated with the accuracy order not lower than 4th order, the Taylor expansion analysis of (9) and (10) will give the following relation[31, 32],

$$\frac{1}{\Delta\xi}(\tilde{R}_{i+1/2} - \tilde{R}_{i-1/2}) = R^{'}(\xi_i) + O(\Delta\xi^4) \tag{12}$$

i.e. the 4th order accuracy is achieved. It needs to point out that in Eq.(9), $\tilde{R}_{i-1/2}$ can not be replaced by $R_{i-1/2}$. Otherwise, the 4th order accuracy can not be achieved even though the high order approximation of $R_{i-1/2}$ is used.

In order to achieve the highest order accuracy of R_I with $I = i-3/2, i-1/2, i+1/2$, the approximation of each component in Eq. (10) using all the involved points of the WENO stencil is given below:

$$\mu_I = \sum_{l=m}^{n} C_l^I \mu_{i+l}, \tag{13}$$

$$\frac{\partial u}{\partial \xi}|_I = \frac{1}{\Delta\xi} \sum_{l=r}^{s} D_l^I u_{i+l}, \tag{14}$$

$$\frac{\partial u}{\partial \eta}|_I = \sum_{l=m}^{n} C_l^I \frac{\partial u}{\partial \eta}|_{i+l,j} \tag{15}$$

where

$$\frac{\partial u}{\partial \eta}|_{i,j} = \frac{1}{\Delta\eta} \sum_{l=p}^{q} C_l^c u_{i,j+l}, \tag{16}$$

By choosing different ranges for $(m,n),(r,s),(p,q)$ and different coefficients C_l^I, D_l^I, C_l^c, one can obtain different order accuracy approximation to the viscous terms. The principle of choosing $(m,n),(r,s),(p,q)$ is to ensure that the approximation of $\frac{\partial R}{\partial \xi}|_i$ in Eq.(9) is a central differencing. For example, in this paper, $(m,n) = (-2,1),(r,s) = (-3,2), and\ (p,q) = (-2,2)$ are used, and they give[32],

$$\mu_I = \sum_{l=m}^{n} C_l^I \mu_{i+l} + O(\Delta\xi^4), \tag{17}$$

$$\frac{\partial u}{\partial \xi}|_I = \frac{1}{\Delta\xi} \sum_{l=r}^{s} D_l^I u_{i+l} + O(\Delta\xi^5), \tag{18}$$

$$\frac{\partial u}{\partial \eta}|_I = \sum_{l=m}^{n} C_l^I \frac{\partial u}{\partial \eta}|_{i+l,j} + O(\Delta\xi^4, \Delta\eta^4), \tag{19}$$

where

$$\frac{\partial u}{\partial \eta}|_{i,j} = \frac{1}{\Delta\eta} \sum_{l=p}^{q} C_l^c u_{i,j+l} + O(\Delta\eta^4) \tag{20}$$

the coefficients C_l^I, D_l^I, C_l^c can be obtained by Taylor's series expansion and are given in Tables 1-3. For example,

$$\begin{cases} \mu_{i-3/2} = \frac{1}{16}(5\mu_{i-2} + 15\mu_{i-1} - 5\mu_i + \mu_{i+1}) + O(\Delta\xi^4) \\ \mu_{i-1/2} = \frac{1}{16}(-\mu_{i-2} + 9\mu_{i-1} + 9\mu_i - \mu_{i+1}) + O(\Delta\xi^4) \\ \mu_{i+1/2} = \frac{1}{16}(\mu_{i-2} - 5\mu_{i-1} + 15\mu_i + 5\mu_{i+1}) + O(\Delta\xi^4) \end{cases} \tag{21}$$

$$\begin{cases} \frac{\partial u}{\partial \xi}|_{i-3/2} = \frac{1}{\Delta\xi}(\frac{71}{1920}u_{i-3} - \frac{141}{128}u_{i-2} + \frac{69}{64}u_{i-1} + \frac{1}{192}u_i - \frac{3}{128}u_{i+1} + \frac{3}{640}u_{i+2}) + O(\Delta\xi^5) \\ \frac{\partial u}{\partial \xi}|_{i-1/2} = \frac{1}{\Delta\xi}(-\frac{3}{640}u_{i-3} + \frac{25}{384}u_{i-2} - \frac{75}{64}u_{i-1} + \frac{75}{64}u_i - \frac{25}{384}u_{i+1} + \frac{3}{640}u_{i+2}) + O(\Delta\xi^5) \\ \frac{\partial u}{\partial \xi}|_{i+1/2} = \frac{1}{\Delta\xi}(-\frac{3}{640}u_{i-3} + \frac{3}{128}u_{i-2} - \frac{1}{192}u_{i-1} - \frac{69}{64}u_i + \frac{141}{128}u_{i+1} - \frac{71}{1920}u_{i+2}) + O(\Delta\xi^5) \end{cases} \tag{22}$$

The other terms are determined similarly.

Table 1: The coefficients of C_l^I

I	C_{-2}^I	C_{-1}^I	C_0^I	C_1^I
$i-3/2$	5/16	15/16	-5/16	1/16
$i-1/2$	-1/16	9/16	9/16	-1/16
$i+1/2$	1/16	-5/16	15/16	5/16

Table 2: The coefficients of D_l^I

I	D_{-3}^I	D_{-2}^I	D_{-1}^I	D_0^I	D_1^I	D_2^I
$i-3/2$	71/1920	-141/128	69/64	1/192	-3/128	3/640
$i-1/2$	-3/640	25/384	-75/64	75/64	-25/384	3/640
$i+1/2$	-3/640	3/128	-1/192	-69/64	141/128	-71/1920

Table 3: The coefficients of C_l^c

C_{-2}^c	C_{-1}^c	C_0^c	C_1^c	C_2^c
1/12	-8/12	0	8/12	-1/12

Ref. [32] proved that the scheme of Eq. (9) is symmetric with respect to cell i and is of 4th-order accuracy. The symmetry of Eq. (9) satisfies the diffusion property of viscous fluxes.

5 Time Marching Method

The implicit fluxes given in Eq. (4) are treated as the following. The inviscid fluxes defined by Eq. (4) are expanded in Taylor's series about interface $i+1/2$,

$$E^L_{i+1/2}|^{n+1} = E^L_{i+1/2}|^n + (\frac{\partial E}{\partial q}|^L_{i+1/2})|^n \Delta q^L_{i+1/2}|^{n+1}$$
$$= E^L_{i+1/2}|^n + A^L_{i+\frac{1}{2}}|^n \Delta q^L_{i+1/2}|^{n+1}$$
$$E^R_{i+1/2}|^{n+1} = E^R_{i+1/2}|^n + (\frac{\partial E}{\partial q}|^R_{i+1/2})|^n \Delta q^R_{i+1/2}|^{n+1}$$
$$= E^R_{i+1/2}|^n + A^R_{i+\frac{1}{2}}|^n \Delta q^R_{i+1/2}|^{n+1}$$

and,

$$\tilde{A}(q^R - q^L)|^{n+1}_{i+1/2} =$$
$$\tilde{A}(q^R - q^L)|^n_{i+1/2} + \tilde{A}_{i+1/2}|^n (\Delta q^R_{i+1/2}|^{n+1} - \Delta q^L_{i+1/2}|^{n+1})$$

The first-order approximation is used for the implicit convective terms to enhance diagonal dominance. That is:

$$\Delta q^L_{i+1/2}|^{n+1} = \Delta q^{n+1}_i, \quad \Delta q^R_{i+1/2}|^{n+1} = \Delta q^{n+1}_{i+1}$$

The fluxes F and G are treated in the same way. The implicit viscous fluxes R, S and T are discretized using 2nd order central differencing. Then the final implicit form is the following,

$$\bar{B}\Delta q^{n+1}_{i,j,k} + A^+ \Delta q^{n+1}_{i+1,j,k} + A^- \Delta q^{n+1}_{i-1,j,k} + B^+ \Delta q^{n+1}_{i,j+1,k} + B^- \Delta q^{n+1}_{i,j-1,k} +$$
$$C^+ \Delta q^{n+1}_{i,j,k+1} + C^- \Delta q^{n+1}_{i,j,k-1} = RHS^n \tag{23}$$

The Gauss-Seidel line iteration in a certain sweep direction, for example, in ξ direction assuming the sweeping from small index value to large one, can be written as

$$B^- \Delta q^{n+1}_{i,j-1,k} + \bar{B}\Delta q^{n+1}_{i,j,k} + B^+ \Delta q^{n+1}_{i,j+1,k} = RHS' \tag{24}$$

where,

$$RHS' = RHS^n - A^+ \Delta q^n_{i+1,j,k} - A^- \Delta q^{n+1}_{i-1,j,k} - C^+ \Delta q^n_{i,j,k+1} - C^- \Delta q^{n+1}_{i,j,k-1} \tag{25}$$

6 Results and Discussion

To demonstrate the effectiveness of the high order preconditioning methodlofy, the test cases include a cavity natural convection flow, a subsonic flat plate turbulent boundary layer, inviscid transonic converging-diverging nozzle flow, the transonic flow over RAE2822 airfoil, and the laminar wall boundary layer with Mach number from 10^{-3} to 2.0.

6.1 Cavity Natural Convection Flow

The first test case is a cavity natural convection flow induced by a temperature difference of 4 times on the two vertical walls. This flow has very low velocity and is completely in the incompressible flow regime. The configuration consists of two insulated horizontal walls and two vertical walls at temperature T_h and T_c, $T_h = 4T_c$. A 100×100 uniform grid is used. In this paper, the natural convective flows at two Rayleigh number, $Ra = 10^3$ and $Ra = 10^5$, are calculated.

Excellent convergences are obtained as shown in Fig. 1 with $CFL = 5.0$. Figs. 2-5 show the stream-

line and temperature isolines. The preconditioning is critical as mentioned in the introduction for these incompressible low speed flows to remove the stiffness so that the simulation can converge, and to reduce the numerical dissipation of a Riemann solver at low flow speed. Fig. 6 is temperature isolines of $Ra = 10^5$ with a finer mesh 200×200.

6.2 Wall Boundary Layer

The second case is a steady state laminar boundary layer flow on an adiabatic flat plate to test the methodology for both compressible and incompressible flows. The Reynolds number based on the length of the flat plate is 4.0×10^4. The Prandtl number of 1.0 is used in order to compare with the analytical solution. The computation domain is taken to be $[0, 2] \times [0, 1.6]$. The mesh size is 180×80.

Three cases with different incoming Mach number are calculated:

(1). $M = 2.0$, $CFL = 1000$;

(2). $M = 10^{-2}$, $CFL = 10$;

(3). $M = 10^{-3}$, $CFL = 10$.

Fig. 9 is the convergence histories of case (1) with Mach number of 2.0, the supersonic flat plate laminar flow, with and without preconditioning. It shows that the precondition method has the same convergence rate as the one without preconditioning. For this supersonic flow, the thin subsonic boundary layer has created little stiffness and hence the advantage of preconditioning is not significant.

The velocity and temperature profiles of case (1) shown in Figs. 8 and **??** indicate that the numerical results agree excellently with the Blasius solution.

Figs. 10 and 11 show the convergence histories of the cases with $M = 10^{-2}$ and $M = 10^{-3}$. It can be seen that the residuals of the two cases do not reach machine zero as other examples. This is explained by Choi and Merkle[7] due to the reason that, for low Mach number computations, the decreasing Mach number results in the increased machine roundoff errors. It was shown that roundoff error begins to dominate below $M = 10^{-3}$ and it increases proportionally with M^2. The cause of this roundoff error arises from the calculation of pressure gradients. Using a gauge pressure is suggested to circumvent this problem,

$$p = \bar{p} + p' \tag{26}$$

where $\bar{p}$ is the gauge pressure and is an arbitrary constant. The fluxes q, E, F and G then should be redefined by using Eq. (26)[7].

In our computations, no gauge pressure treatment is used in order to have a fair comparison of the convergence history. Figs. 10 and 11 indicate that the preconditioning solver drive the residual several orders of magnitude lower that the one without preconditioning.

Figs. 12 and 13 are the comparisons of numerical results with Blasius solution for $M = 10^{-2}$ and 10^{-3}. Figs. 12 shows that the flow solver without preconditioning can still accurately resolve the boundary layer at $M = 10^{-2}$. However, the velocity profile in Fig. 13 demonstrates that, for the case with $M = 10^{-3}$, the numerical solution without preconditioning is significantly diffused due to the large numerical dissipation, whereas the preconditioned solvers accurately resolve the velocity profile.

6.3 Subsonic Flat Plate Turbulent Boundary Layer

A subsonic flat plate turbulent boundary layer is used to test the methodology with a RANS turbulence model in compressible flow regime. The inlet Mach number is 0.5 and the Reynolds number is 4×10^6 based on the plate length. The computation domain is taken to be $[0, 1] \times [0, 1]$. The mesh size is 180×80.

The non-dimensional distance y^+ of the first grid point to the wall is kept under 0.2. The Baldwin-Lomax turbulence model is used. The flow is subsonic at inlet and outlet. The CFL number of 200 is used.

The convergence histories are shown in Fig. 14 for both with and without preconditioning. It can be seen that with preconditioning, the convergence rate is about 30% more efficient to drive the residual to machine zero. The faster convergence may be attributed to the improved condition in the near wall incompressible flow region.

Fig. 15 shows that both the results with and without preconditioning are identical and agree well with the law of the wall.

6.4 Transonic Converging-Diverging Nozzle

To examine the performance of the preconditioning methodology in two-dimensional flow and the capability to capture shock waves, an inviscid transonic converging-diverging nozzle is calculated. The nozzle was designed and tested at NASA and was named as Nozzle A1[33]. Due to the geometric symmetry about the center line, only the upper half of the nozzle is calculated. The mesh size is 175×50. The grid is clustered near the wall. The inlet Mach number is 0.22. The CFL number of 5 is used.

Fig. 16 shows the Mach contours obtained by present preconditioning method. Fig. 17 is the comparison of the convergence histories with and without precondition. Similar to the flow of subsonic flat plate turbulent boundary layer, the preconditioned convergence rate is again about 30% faster than the one without preconditioning.

Fig. 18 shows the pressure coefficients at the upper wall surface. It can be seen that both the methods with and without preconditioning obtain identical results.

Figs. 19 and 20 are the convergence history and the pressure coefficients distribution with a finer mesh of 350×100. Same as the conclusion of coarse mesh 175×50, the preconditioned calculation is about 30% faster than the one without preconditioning.

6.5 Transonic RAE2822 Airfoil

To further examine the preconditioning method for transonic compressible flows, the steady state solution of the transonic RAE2822 airfoil is calculated using the Reynolds averaged Navier-Stokes equations with the Baldwin-Lomax turbulence model. The mesh size is 256×55, the freestream Mach number M_∞ is 0.729, the Reynolds number based on chord is 6.5×10^6, and the angle of attack is 2.31^o.

Fig. 21 shows the Mach contours obtained by present preconditioning method.

Again, from Fig. 22, we can see that the preconditioning method only needs about half of the iteration numbers of the one without preconditioning to converge to machine zero.

Fig. 23 shows that both the results with and without preconditioning are identical and are in good agreement with the experiment.

7 Conclusions

An unified algorithm is developed in this paper to calculate flow fields from very low speed incompressible flows to supersonic compressible flows. The preconditioning matrix of Weiss and Smith combined with a 5th-order WENO scheme for inviscid flux and a fully conservative 4th order central differencing for viscous terms are employed. The unfactored implicit Gauss-Seidel relaxation scheme is used for time marching.

The numerical simulation of a natural convective incompressible cavity flow, low subsonic incompressibe flows, transonic and supersonic compressible flows show that the preconditioning method is efficient, accurate and robust, not only for the low Mach number incompressible flows, but also for the subsonic and transonic compressible flows. For high subsonic and transonic flows, the preconditioning also accelerates convergence due to reduced stiffness in near wall low speed region. For low speed incompressible flows, the preconditioning is necessary not only to remove the stiffness, but also to reduce numerical dissipation to ensure accurate results. Mesh refinement study is done for two selected cases, the natural convective incompressible flow and the transonic nozzle flow. The suggested algorithm achieves excellent convergence for both cases.

8 Acknowledgment

This work is supported by Miami Wind ^{TM} Research Center at University of Miami.

References

[1] A. L. De Bortoli, "Multigrid based aerodynamical simulations for the NACA 0012 airfoil," *Applied Numerical Mathematics*, vol. 40, pp. 337–349, 2002.

[2] S. Polsky, "Progress Towards Modeling Ship/Aircraft Dynamic Interface." hpcmp-ugc,pp.163-168, HPCMP Users Group Conference (HPCMP-UGC'06), 2006.

[3] Niles A. Pierce, Michael B. Giles, "Preconditioned Multigrid Methods for Compressible Flow Calculations on Stretched Meshes," *Journal of Computational Physics*, vol. 136, pp. 425–445, 1997.

[4] E. Turkel, "Preconditioned methods for solving the incompressible and low speed compressible equations," *Journal of Computational Physics*, vol. 72, pp. 277–298, 1987.

[5] C.L. Merkle, Y.H. Choi, "Computation of low-speed compressible flows with time-marching procedures," *International Journal for Numerical Methods in Engineering*, vol. 25, pp. 293–311, 1988.

[6] E. Turkel, "Preconditioning techniques in computational fluid dynamics," *Annu. Rev. Fluid Mech.*, vol. 31, pp. 385–416, 1999.

[7] Y. Choi and C. Merkle, "The Application of Preconditioning in Viscous Flows," *Journal of Computational Physics*, vol. 105, pp. 207–223, 1993.

[8] J.M. Weiss, and W.A. Smith, "Preconditioning Applied to Variable and Constant Density Flows," *AIAA Journal*, vol. 33, pp. 2050–2057, 1995.

[9] E. Turkel, "Review of preconditioning methods for fluid dynamics," *Applied Numerical Mathematics*, vol. 12, pp. 257–284, 1993.

[10] N. Alkishriwi, M. Meinke, W. Schroder, "A large-eddy simulation method for low Mach number flows using preconditioning and multigrid," *Computers & Fluids*, vol. 35, pp. 1126–1136, 2006.

[11] Z.F. Xu and C.-W. Shu, "Anti-diffusive flux corrections for high order finite difference WENO schemes," *J.Comput.Phys.*, vol. 205, pp. 458–485, 2005.

[12] R.C. Swanson, E. Turkel, C.-C. Rossow, "Convergence acceleration of Runge-Kutta schemes for solving the Navier-Stokes equations," *Journal of Computational Physics*, vol. 224, pp. 365–388, 2007.

[13] S. Yamamoto, "Preconditioning method for condensate fluid and solid coupling problems in general curvilinear coordinates," *Journal of Computational Physics*, vol. 207, pp. 240–260, 2005.

[14] C.L. Merkle, J.Y. Sullivan, P.E.O. Buelow and S. Venkateswaran, "Computation of Flows with Arbitrary Equations of State," *AIAA Journal*, vol. 36, pp. 515–521, 1998.

[15] J.M. Weiss, J.P. Maruszewski, W.A. Smith, "Implicit solution of preconditioned Navier-Stokes equations using algebraic multigrid," *AIAA Journal*, vol. 37, pp. 29–36, 1999.

[16] C. -C. Rossow, "Efficient computation of compressible and incompressible flows," *Journal of Computational Physics*, vol. 220, pp. 879–899, 2007.

[17] W. R. Briley, L. K. Taylor, D. L. Whitfield, "High-resolution viscous flow simulations at arbitrary Mach number," *Journal of Computational Physics*, vol. 184, pp. 79–105, 2003.

[18] E. Turkel, R. Radespiel, N. Kroll, "Assessment of preconditioning methods for multidimensional aerodynamics," *Computers & Fluids*, vol. 26, pp. 613–634, 1997.

[19] J.R. Edwards,M.-S. Liou, "Low-Diffusion Flux-Splitting Methods for Flows at All Speeds," *AIAA Journal*, vol. 36, pp. 1610–1617, 1998.

[20] N. Nigro, M. Storti, S. Idelsohn, T. Tezduyar, "Physics based GMRES preconditioner for compressible and incompressible Navier-Stokes equations," *Computer Methods in Applied Mechanics and Engineering*, vol. 154, pp. 203–228, 1998.

[21] C. -C. Rossow, "A blended pressure/density based method for the computation of incompressible and compressible flows," *Journal of Computational Physics*, vol. 185, pp. 375–398, 2003.

[22] X.D. Liu, S. Osher, and T. Chan, "Weighted essentially non-oscillatory schemes," *J.Comput.Phys.*, vol. 115, pp. 200–212, 1994.

[23] G.S. Jiang, and C.W. Shu, "Efficient implementation of weighted ENO schemes," *J.Comput.Phys.*, vol. 126, pp. 202–228, 1996.

[24] A.C. Taylor III, W.F. Ng, R.W. Walters, "An improved upwind finite volume relaxation method for high speed viscous flows," *J.Compu.Phys.*, vol. 99, pp. 159–168, 1992.

[25] S.E. Rogers, F.R. Menter, N.N. Mansour, and P.A. Durbin, "A comparison of turbulence models in computing multi-element airfoil flows." AIAA 94-0291, Jan. 1994.

[26] L. Yuan, "Comparison of implicit multigrid schemes for three-dimensional incompressible flows," *J. Compu. Phys.*, vol. 177, pp. 134–155, 2002.

[27] Y.Q. Shen, B.Y. Wang,and G.C. Zha, "Comparison Study of Implicit Gauss-Seidel Line Iteration Method for Transonic Flows." AIAA-paper 2007-4332, June 2007.

[28] B. Baldwin and H. Lomax, "Thin Layer Approximation and Algebraic Model for Separated Turbulent Flows." AIAA Paper 78-257, 1978.

[29] P. Roe, "Approximate Riemann Solvers, Parameter Vectors, and Difference Schemes," *Journal of Computational Physics*, vol. 43, pp. 357–372, 1981.

[30] B. Van Leer, "Towards the Ultimate Conservative Difference Scheme, III," *Journal of Computational Physics*, vol. 23, pp. 263–75, 1977.

[31] Y.Q. Shen, B.Y. Wang,and G.C. Zha, "Implicit WENO scheme and high order viscous formulas for compressible flows." AIAA-paper 2007-4431, June 2007, to appear in AIAA Journal.

[32] Y. Q. Shen, G. -C. Zha, X. Y. Chen, " High Order Conservative Differencing for Viscous Terms and the Application to Vortex-Induced Vibration Flows." AIAA-2008-4059, 2008.

[33] M. L. Mason and L. E. Putnam, "The Effect of Throat Contouring on Two-Dimensional Converging-Diverging Nozzles at Static Conditions ." NASA Technical Paper 1704, 1980.

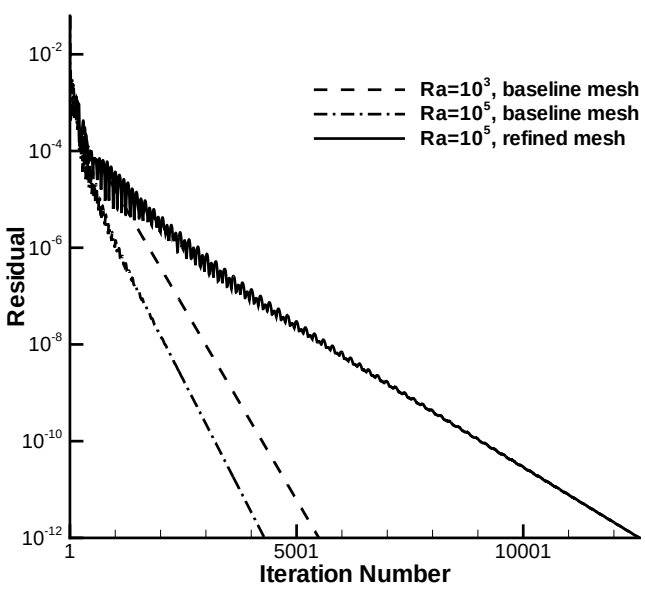

Figure 1: Convergence histories of the cavity natural convection flows.

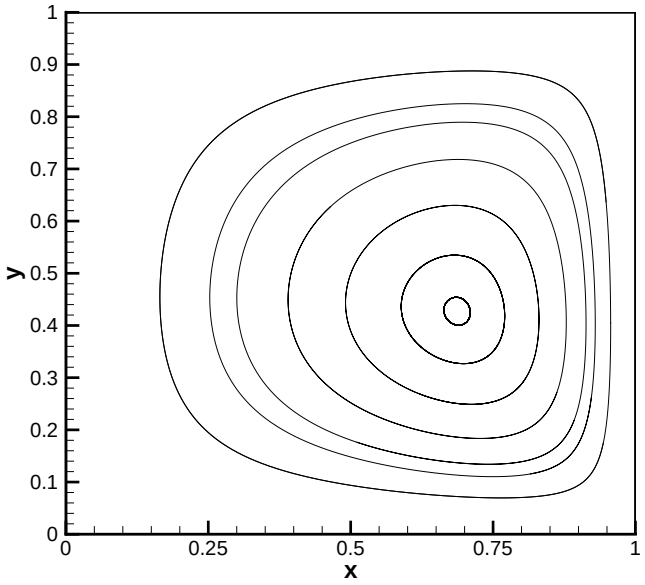

Figure 2: Streamline of the cavity natural convection flow, $Ra = 10^3$.

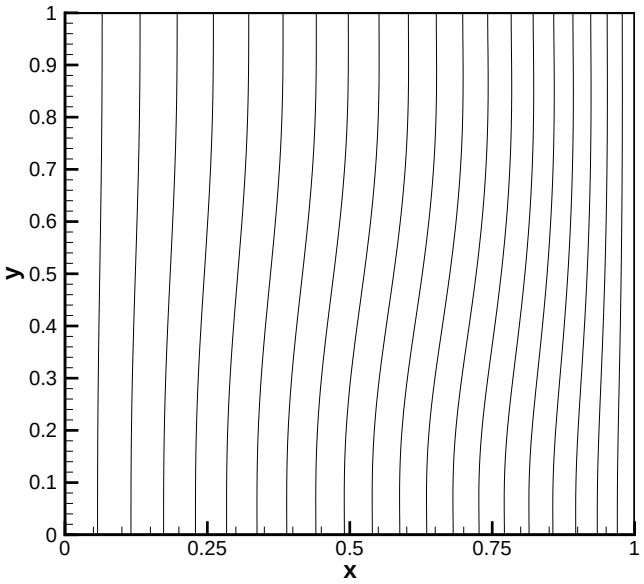

Figure 3: Isoline temperature of the cavity natural convection flow, $Ra = 10^3$.

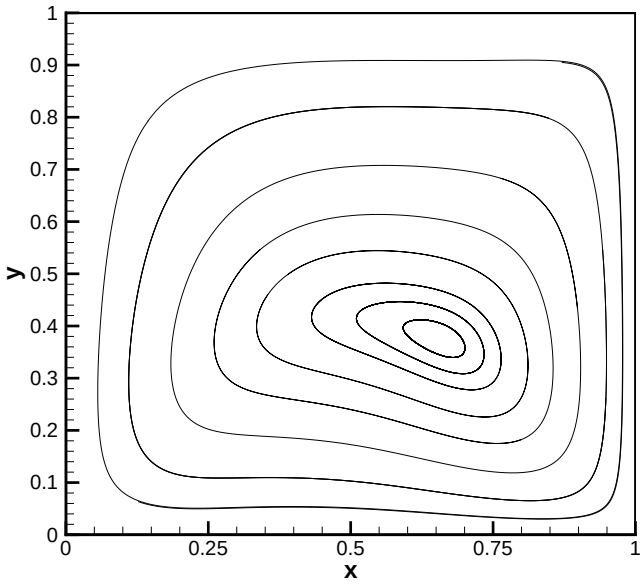

Figure 4: Streamline of the cavity natural convection flow, $Ra = 10^5$.

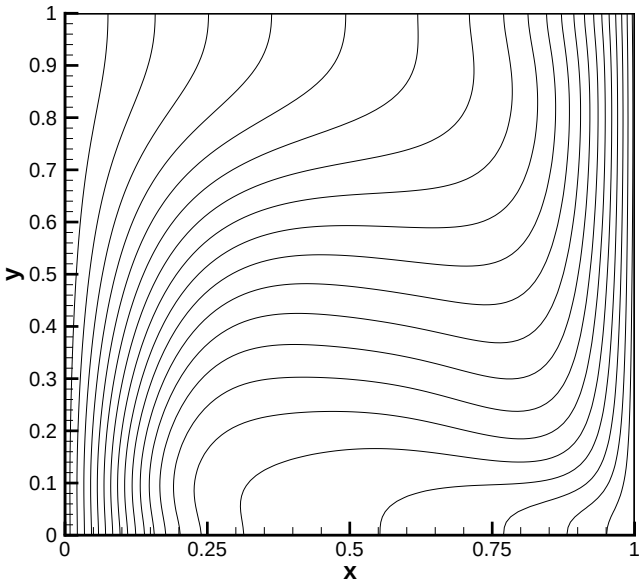

Figure 5: Isoline temperature of the cavity natural convection flow, baseline mesh, $Ra = 10^5$.

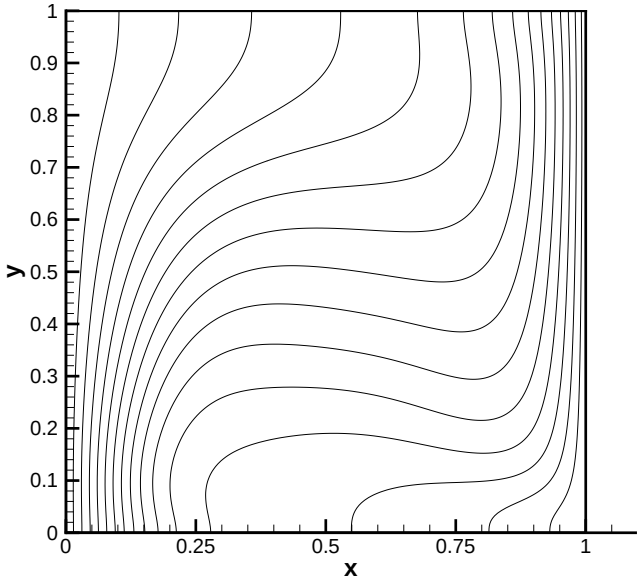

Figure 6: Isoline temperature of the cavity natural convection flow, refined mesh of 200×200, $Ra = 10^5$.

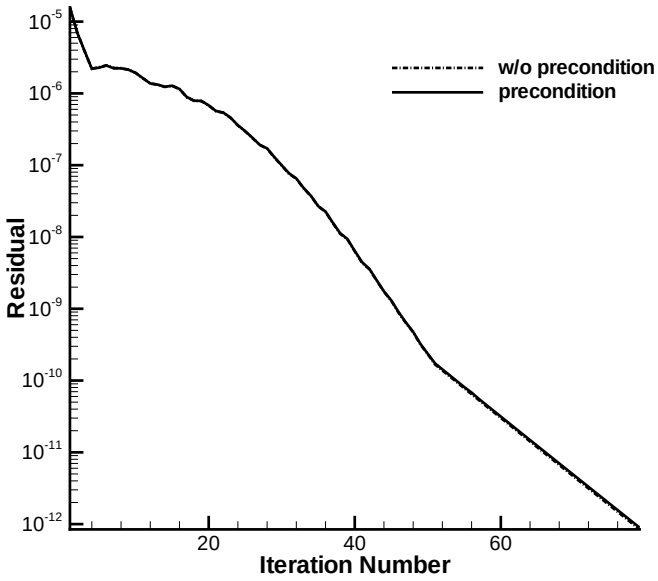

Figure 7: Convergence histories of the supersonic boundary layer flow, $M = 2.0$.

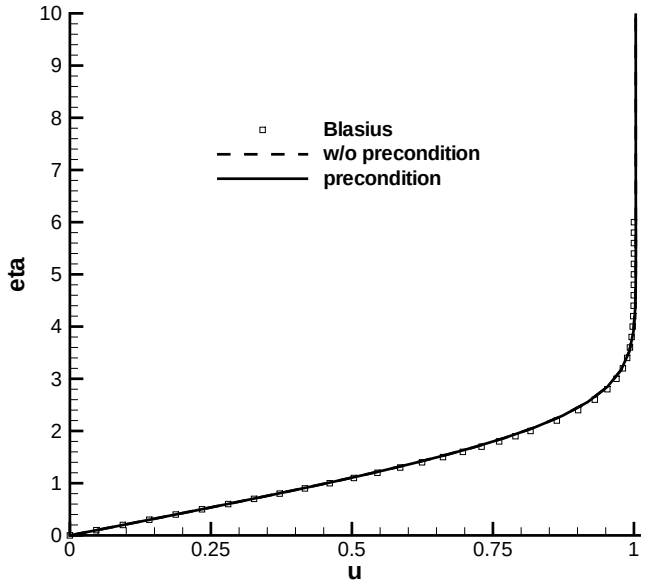

Figure 8: Velocity profile of the supersonic boundary layer flow, $M = 2.0$.

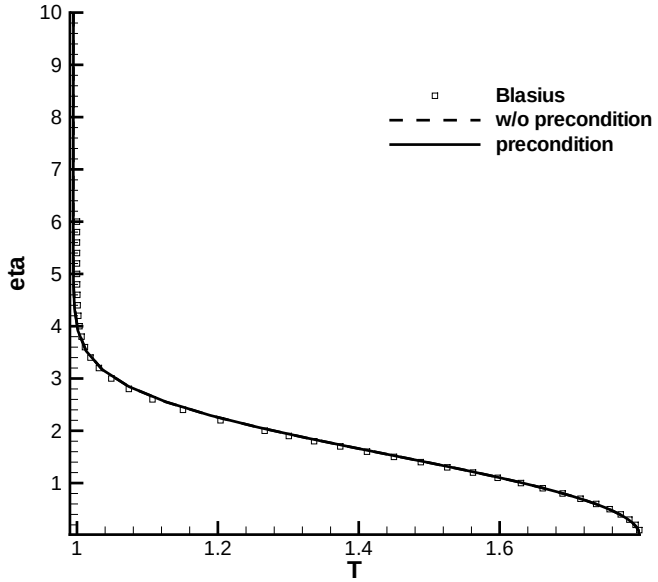

Figure 9: Temperature profile of the supersonic boundary layer flow, $M = 2.0$.

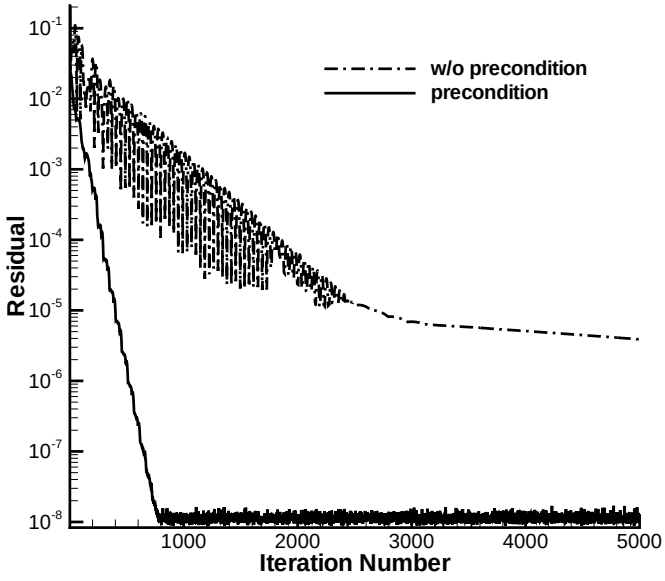

Figure 10: Convergence histories of the subsonic boundary layer flow, $M = 10^{-2}$.

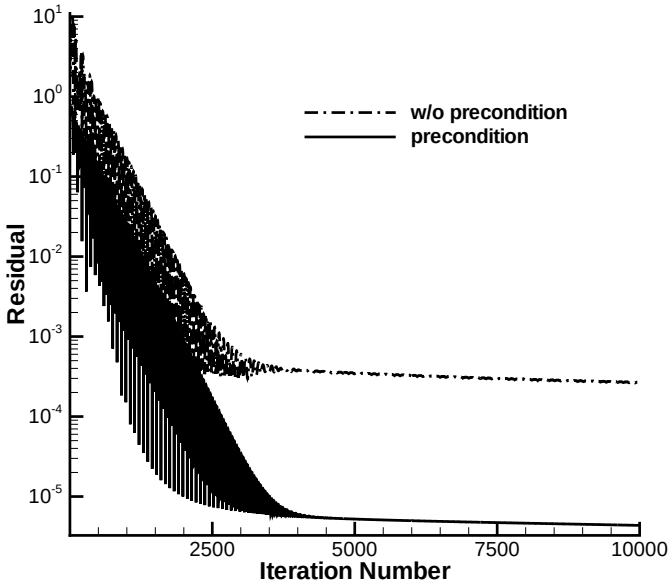

Figure 11: Convergence histories of the subsonic boundary layer flow, $M = 10^{-3}$.

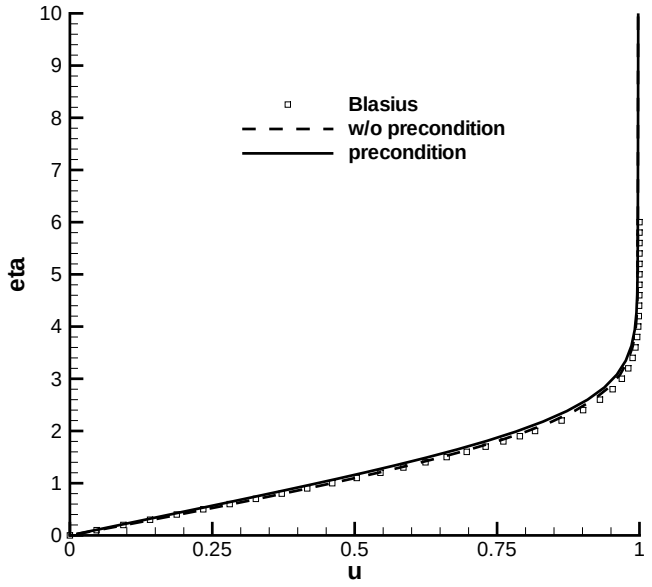

Figure 12: Velocity profile of the subsonic boundary layer flow, $M = 10^{-2}$.

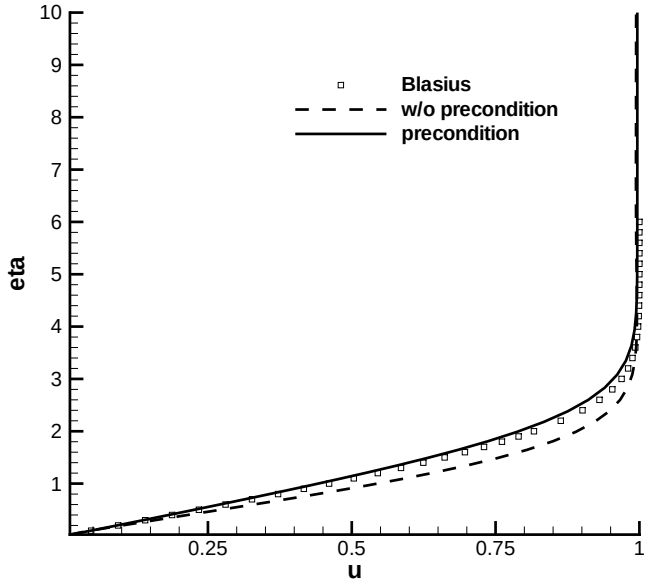

Figure 13: Velocity profile of the subsonic boundary layer flow, $M = 10^{-3}$.

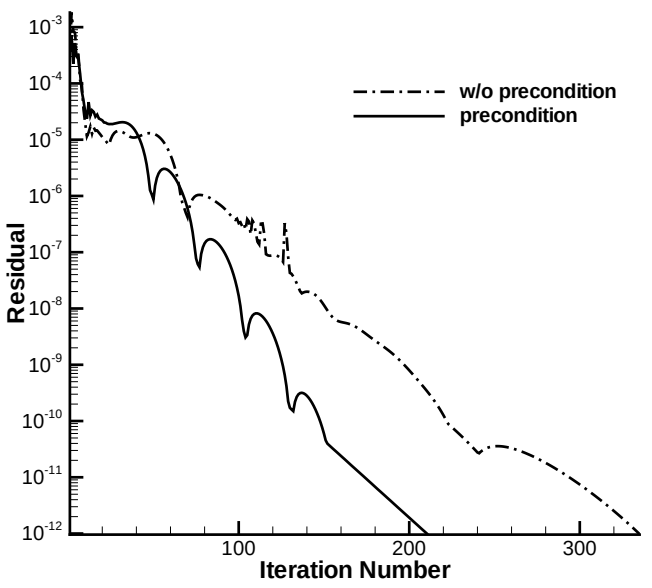

Figure 14: Convergence histories of subsonic flat plate turbulent boundary layer.

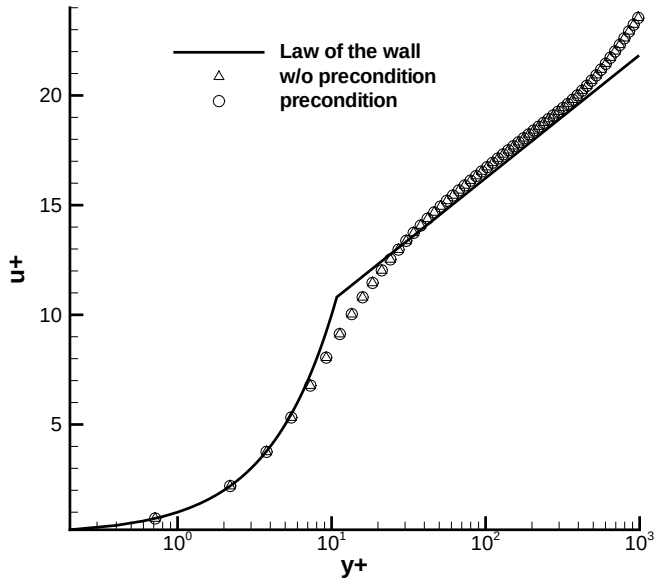

Figure 15: Velocity profile of turbulent boundary layer.

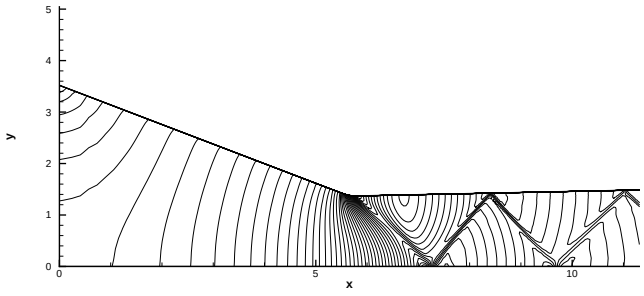

Figure 16: Mach contours of the transonic converging-diverging nozzle flow.

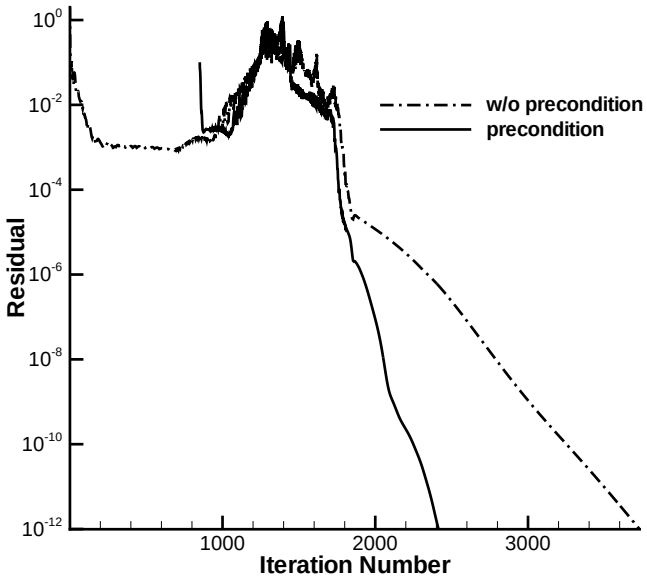

Figure 17: Convergence histories of the transonic converging-diverging nozzle flow.

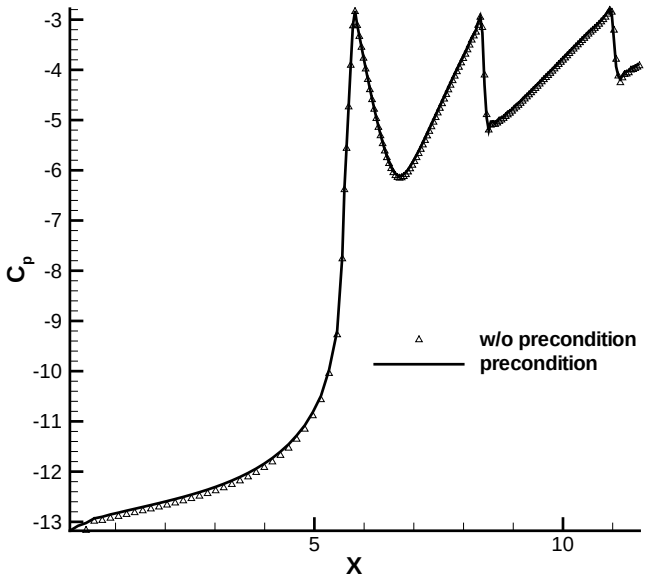

Figure 18: The pressure coefficients at the upper wall of the transonic converging-diverging nozzle flow.

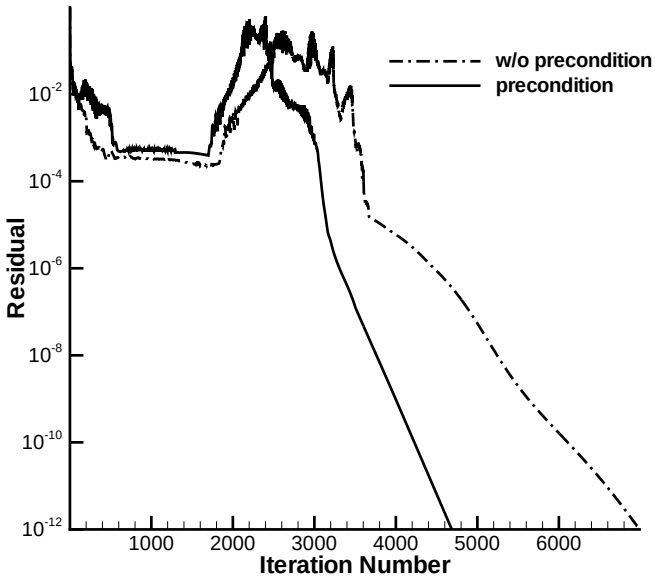

Figure 19: Convergence histories of the transonic converging-diverging nozzle flow, 350×100.

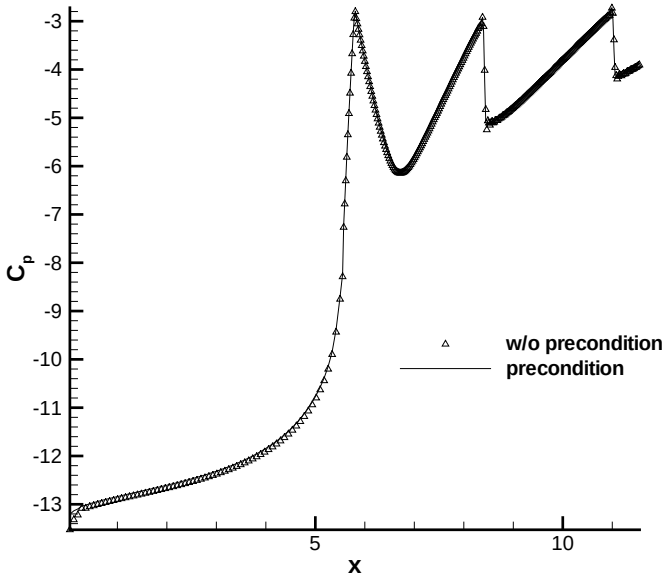

Figure 20: The pressure coefficients at the upper wall of the transonic converging-diverging nozzle flow, 350×100.

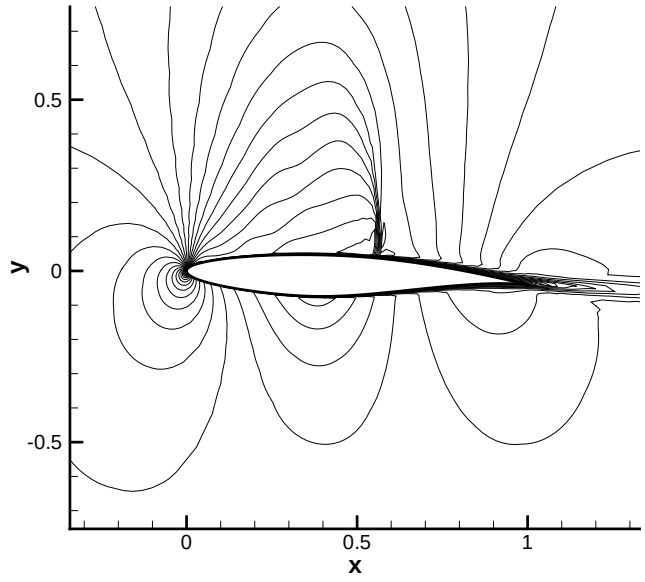

Figure 21: Mach contours of the transonic flow over RAE2822 airfoil.

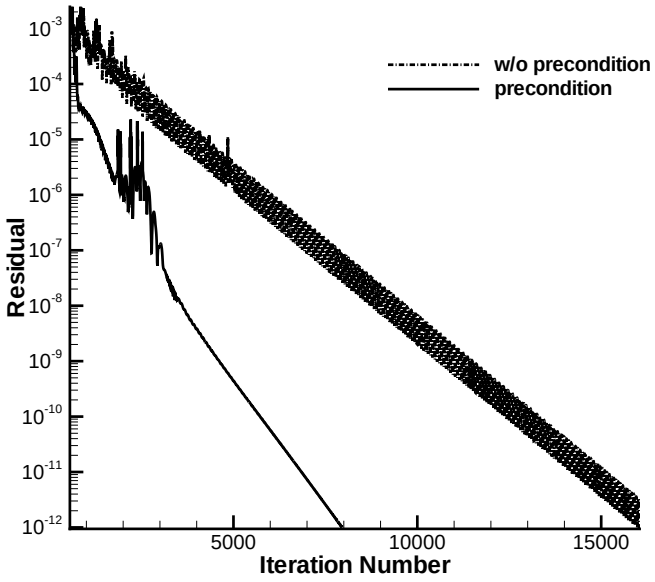

Figure 22: Convergence histories of the transonic flow over RAE2822 airfoil.

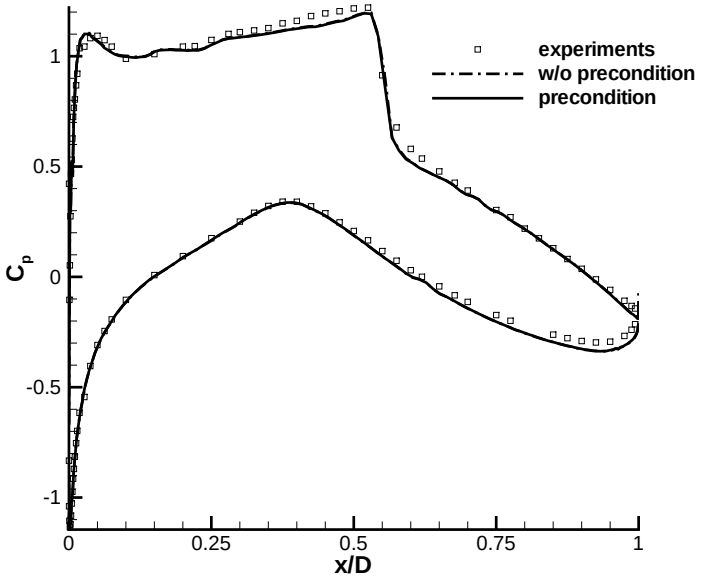

Figure 23: The pressure coefficients at the airfoil surface of the transonic flow over RAE2822 airfoil.